Radar-Based Radial Arterial Pulse Rate and Pulse Pressure Analysis

Yu Rong, Kumar Vijay Mishra and Daniel W. Bliss

***Abstract*—In this paper, we investigate the possibility of using remote sensing technique - radar to detect vascular flow changes in peripheral body part, wrist. Unlike computed tomography, X-rays, radars emit very low power, non-ionizing radio frequency signals, and thus have been shown to detect inner organ vibrations previously [1]–[4]. In our radar-based study, we show pulse rate and pulse strength/pressure as a result of radial arterial blood flow changes at wrist can be detected through carefully designed experiments, in which, we mimic reduced blood circulation such as blood clots in one arm by applying variable physical pressure to peripheral artery. Our proposed radar measurements are (negatively-) correlated with the sphygmomanometer pressure readings. Our results indicate that radar is a potential non-invasive sensing technology to detect vascular flow changes in prevention of peripheral artery diseases.**

***Index Terms*—FMCW radar, remote sensing, wrist palpation, pulse detection**

I. Introduction

The vascular system, also referred as the circulatory system, is made of the vessels that carry blood and other essential body fluids through the body. Blood moves through the circulatory system as a result of being pumped out by the heart.

Also, the vascular system functions as an important component of other body systems, such as respiratory system, digestive system. It is vital important to be able to monitor vascular blood flow [5]. Organs and other body structures may be damaged by vascular disease as a result of decreased or completely blocked blood flow. The causes of vascular disease are found not uncommon among people, such as blood clots, inflammation, trauma and so on. Physical surgeries can change blood circulation as well.

II. Related Works

There are a few techniques available for vascular health monitoring. Computed tomography (CT) angiography [6] uses an injection of contrast material into the blood vessels and the CT scans provide blood flow images. However, the invasive nature gives a painful experience for users. Medical Doppler ultrasonography [7] is a non-invasive alternative that can be used to estimate blood flow through the body by bouncing sound waves off circulating red blood cells, but it requires direct physical contact. Similarly, laser Doppler-based methods [8] and, later, laser specke-based methods [9] are widely exploited for microcirculation analysis. But in general lasers cannot penetrate through clothes. Another promising technology is Terahertz wave [10] because of its attractive characteristics and interactions with tissues. High cost is one obvious issue that hinders Terahertz detection and imaging for large-scale use in near future.

In this paper, we focus on cost-effective and commercial available radio frequency (RF) sensors. A Frequency-Modulated Continuous Wave (FMCW) radar unit is considered in our study. Relatively high carrier frequency (77 GHz) gives good phase sensitivity. Relatively large bandwidth and multiple-input multiple-output (MIMO) array allow target/signal isolation via advanced signal processing techniques. Additionally, radar sensors have some desired features such non-invasive, non-contact, non-ionizing, material penetration, privacy preserving, which are not available in existing medical sensing techniques aforementioned. We exploit these facts and show that by analyzing reflected radar signal from the peripheral body parts the variations in blood flow are detected in a controlled environment, which mimics reduced/blocked blood flow in vascular diseases.

III. Novel Contributions

Our major contributions in microwave-based remote sensing for peripheral vascular blood flow studies lie in twofold:

- We proposed to use micro-vessel motion, which can be reliably and remotely measured by radar sensors, to characterize blood flows in peripheral body parts. As more blood travels through vessels to/from the heart driven by cardiac cycles, the stronger micro-vessel motion (or pressure) is observed; and vise versa.
- We carefully designed three experiments to validate the proposed methodology; experiment 1: detecting radial arterial pulse wave; experiment 2: demonstrating radar pulse rate variability measurement when the test subject was cooling down right after physical exercise; experiment 3: demonstrating radar blood flow variability measurement at wrist when controlled variable pressure was applied to the same upper arm over a period of time.

IV. Micromotion Detection in FMCW Radar

We consider a sawtooth waveform of the FMCW signal in Fig. 2. The transmitted frequency increases with sweep time (T). The initial frequency is f_c and the maximum frequency is bounded by the signal bandwidth (B). A chirp rate is defined as a speed of the frequency change, which is a constant

Y. R. and D. W. B. are with Center for Wireless Information Systems and Computational Architectures (WISCA) at the School of Electrical, Computer and Energy Engineering, Arizona State University, Tempe, AZ 85281 USA, e-mail: yrong5@asu.edu.

K. V. M. is with the United States Army Research Laboratory, Adelphi MD, 20783 USA. E-mail: kumarvijay-mishra@uiowa.edu.

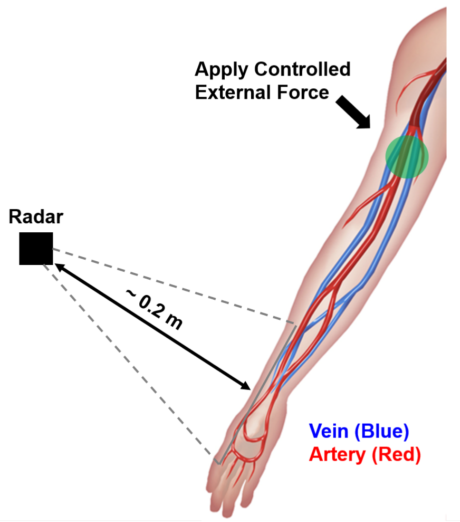

Fig. 1. A sketch of experiment setup. Radar is used to detect radial arterial blood flow changes caused by the controlled external forces.

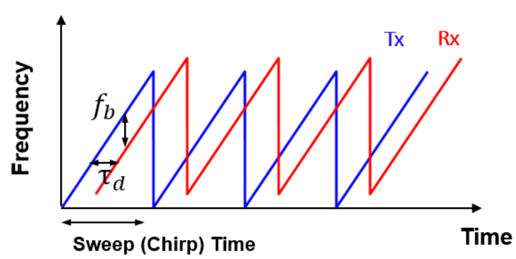

Fig. 2. FMCW sawtooth signal model.

α within T, $\alpha = B/T$. The transmitted periodic linearly-increasing sawtooths are described as,

$$x_{T_x}(\tau) = A_{T_x}\cos\left[2\pi f_c\tau + \pi\alpha\tau^2 + \varphi_0\right], \tag{1}$$

where A_{T_x} is the transmitted power and φ_0 is considered to be the initial phase of the signal. The receiver signal is an attenuated and delayed version of the transmitted sawtooth,

$$x_{R_x}(\tau) = A_{R_x}\cos\left[2\pi f_c(\tau-\tau_d(t)) + \pi\alpha(\tau-\tau_d(t))^2 + \varphi_0\right], \tag{2}$$

where A_{R_x} captures the round-trip pathloss and target response. Two different time scales are used fast-time τ and slow-time t. The first one is used for inter-chirp processing, measuring time of flight and range profile. The latter one is used for intra-chirp processing, measuring Doppler and velocity. $\tau_d(t) = 2D(t)/c = 2(D_0 + D_p(t))/c$ denotes the range and slow-time dependent time-varying delay, where D_0 denotes the nominal radial distance to the target, $D_p(t)$ skin motion related to arterial pulsation and c speed of light. The received signal is mixed with a copy of the transmitted signal and after filtering, by ignoring the phase noise, the constant terms, and receiver noise, the complex baseband signal is approximated as,

$$y(\tau,t) = A_{R_x}e^{j\left[2\pi\alpha\tau_d(t)\tau + 2\pi f_c\tau_d(t)\right]}. \tag{3}$$

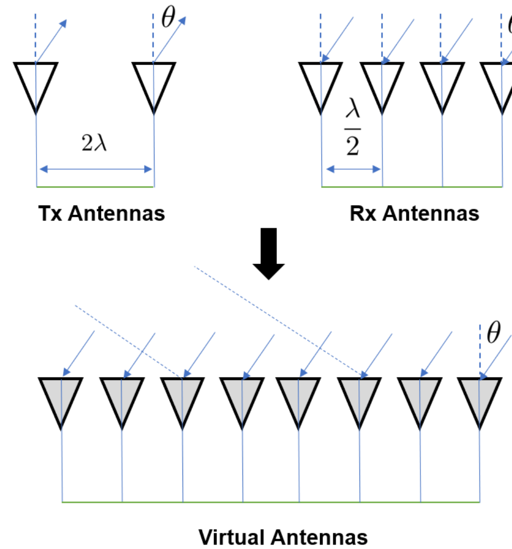

Fig. 3. TDM based MIMO configuration.

If we inspect one chirp by fixing t, the second term in the phasor in Eqn. (3) is simply a constant. The beat frequency $f_b = \alpha\tau_d(t)$ in the first term of the phasor is often used to generate the range profile via fast Fourier Transform (FFT) with repect to τ.

$$y(\nu,t) = A_{R_x}\delta(\nu - f_b)\ e^{j4\pi\frac{D_0+D_p(t)}{\lambda}}, \tag{4}$$

where ν denotes the FFT of t and $\lambda = c/f_c$ is the wavelength. Range bins of interest should be first located via Dirac delta function $\delta(\nu)$ evaluated at f_b before processing applied to t. If a simplified motion model is considered for $D_p(t)$ with physical displacement A_p and repetition frequency f_p, such that $D_p(t) = A_p\sin(2\pi f_p t)$, Eqn. (4) is reduced to,

$$\begin{aligned} y(f_b,t) &= A_{R_x}e^{j\frac{4\pi D_0}{\lambda}}\ e^{j\frac{4\pi A_p\sin(2\pi f_p t)}{\lambda}} \\ &= C\ e^{j\frac{4\pi A_p\sin(2\pi f_p t)}{\lambda}}, \end{aligned} \tag{5}$$

$$\Phi[y(f_b,t)] \sim D_p(t) = A_p\sin(2\pi f_p t), \tag{6}$$

where C encapsulates the terms not dependent on t and $\Phi[\cdot]$ denotes the phase operation. The phase in Eqn. (6) is linearly related to the skin motion.

V. Spatial-Range-Temporal Processings

A. Beamforming

We apply beamforming technique to boost the received signal-to-noise-ratio (SNR). The chirps were transmitted in a time division multiplexing (TDM) MIMO configuration by transmitting sequentially through the transmit (Tx) antennas. Two linearly separated Tx antennas with spacing 2λ and 4-element receive (Rx) array with spacing $\lambda/2$ forms a 8-element virtual array as shown in Fig. (3). For a multiple Rx antenna system, the signal model in Eqn. (3) will accordingly has an additional phase shift representing the phase progression

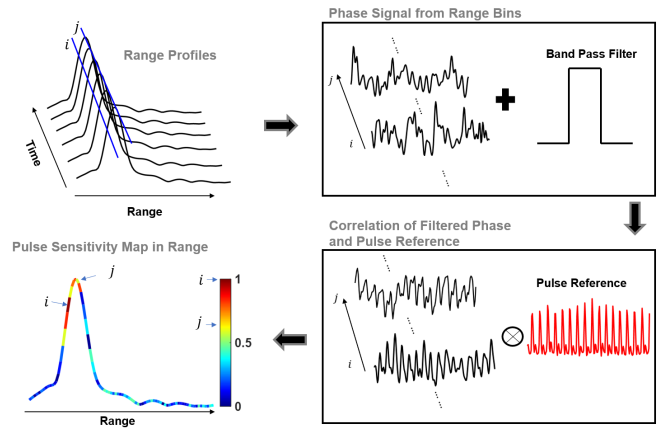

Fig. 4. Process of creating pulse sensitivity map (normalized) overlaid with the range profile.

across the array. For a target at an angle θ, the signal received at the k-th Rx antenna is,

$$y(\tau, t; k) = A_{R_x} e^{j\left[2\pi\alpha\tau_d(t)\tau + 2\pi f_c \tau_d(t)\right]} e^{j\pi(k-1)\sin(\theta)}. \tag{7}$$

We apply steering weights to range FFT results of Eqn. (7) to focus on the targeted range-angle cell. The output of beamformer is,

$$\mathrm{BF}(t) = \sum_k y(\nu = f_b, t; k)\ w_k^*(\theta), \tag{8}$$

where $w_k(\theta) = e^{j\pi(k-1)\theta}$.

B. *Pulse Sensitivity In Range Profile*

We demonstrate the varying pulse sensitivity across range bins in the form of pulse sensitivity map. Usually the stronger reflection point in the range profile is used to locate the target position. However, the pulse signal quality is necessary the best at this single range bin. We propose the pulse sensitivity map to show the motivation of applying multi-channel signal processing to the phase signals from multiple range bins. In order to create the exemplary pulse sensitivity map, we consider 20 seconds radar measurement and 20 seconds pulse reference signal. The temporal phase variation is first extracted from all range bins using Eqn. (6), and then compute the cross-correlation of the extracted phase and the reference pulse signal. Finally, the correlation values are color coded and overlaid with one range profile from the 20 seconds data. The above analysis is illustrated in Figure. 4. The darker the color (dark red) is the higher pulse sensitivity (normalized to unit) is in this range bin, and vice versa.

C. *Multivariate Variational Mode Decomposition (MVMD) Formulation*

MVMD [11] is an multivariate extension of variational mode decomposition (VMD) [12], which has a precise mathematical framework and good mode alignment capability for analyzing multi-channel signals. Previously [13], [14], MVMD has been demonstrated for denoising real-world multivariate dataset with non-stationary nature and low SNR signal recovery in distributed sensor configuration. The MVMD signal model is briefly introduced here and the focus is on how to apply MVMD to this specific problem. The goal of MVMD is to extract predefined O number of multivariate modulated oscillations $\mathbf{u}_o(t)$ from the phase components from a group of range bins (say M) around the peak in the range profile, where the input signals $\mathbf{\Psi}(t) = [p_1(t); p_2(t); ...; p_M(t)]$.

$$\mathbf{\Psi}(t) = \sum_{o=1}^{O} \mathbf{u}_o(t), \tag{9}$$

where $\mathbf{u}_o(t)$ denotes the o-th mode in all channels, $\mathbf{u}_o(t) = [u_{1,o}(t); u_{2,o}(t); ...; u_{M,o}(t)]$. For this particular problem, the underlying signal of interest is pulse-like signal. The input signal $\mathbf{\Psi}(t)$ contains out of band interference and noise. A bandpass filter is first applied to $\mathbf{\Psi}(t)$ and to focus at the relevant frequency bands for pulse. The objective function f for the MVMD optimization problem is to find the solution for Eqn. (9),

$$f = \sum_{o=1} \left|\left|\partial_t \left[\mathbf{u}_o^+(t) e^{-j\omega_o t}\right]\right|\right|_2^2. \tag{10}$$

$\mathbf{u}_o^+(t)$ denotes the vector analytic representation of $\mathbf{u}_o(t)$, and is written as,

$$\mathbf{u}_o^+(t) = \mathbf{u}_o(t) + j\mathcal{H}\mathbf{u}_o(t), \tag{11}$$

where $\mathcal{H}$ denotes Hilbert transform. The motivation for converting to the analytic representation of $\mathbf{u}_o(t)$ being that a multivariate AM-FM vector signal $\mathbf{s}(t)$,

$$\mathbf{s}(t) = \begin{bmatrix} s_1(t) \\ s_2(t) \\ \vdots \\ s_M(t) \end{bmatrix} = \begin{bmatrix} a_1(t)\cos(\theta_1(t)) \\ a_2(t)\cos(\theta_2(t)) \\ \vdots \\ a_M(t)\cos(\theta_M(t)) \end{bmatrix} \tag{12}$$

is not unique since more than one functions for $a_m(t)$ and $\theta_m(t)$ may be associated with real valued $s_m(t)$, which $m = 1, 2, ..., M$. By using analytic representation of $\mathbf{s}(t)$ via Hilbert transformation, a unique canonic set of amplitude and phase functions can be defined, yielding the following complex vector matrix form,

$$\mathbf{s}^+(t) = \begin{bmatrix} s_1^+(t) \\ s_2^+(t) \\ \vdots \\ s_M^+(t) \end{bmatrix} = \begin{bmatrix} a_1(t)e^{j\theta_1(t)} \\ a_2(t)e^{j\theta_2(t)} \\ \vdots \\ a_M(t)e^{j\theta_M(t)} \end{bmatrix} \tag{13}$$

The original real-valued signal vector can be obtained as the real part $\mathcal{R}$ of $\mathbf{s}_+(t)$ as,

$$\mathbf{s}(t) = \mathcal{R}\mathbf{s}^+(t). \tag{14}$$

The constrained optimization problem for MVMD is formally presented as,

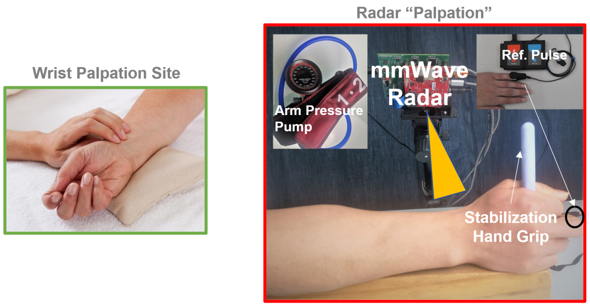

Fig. 5. One snapshot of the experiment scene and used measurement devices.

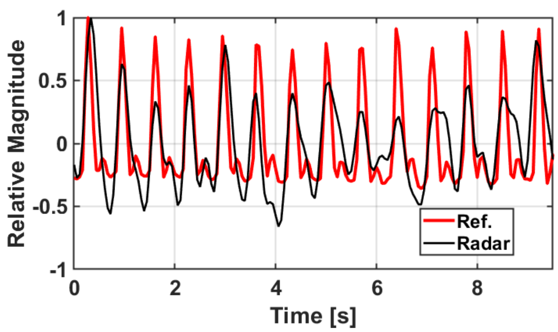

Fig. 6. Radar measured radial arterial pulse waveform.

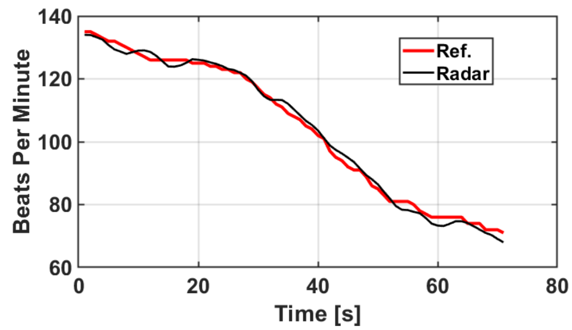

Fig. 7. Radar radial arterial pulse rate variability.

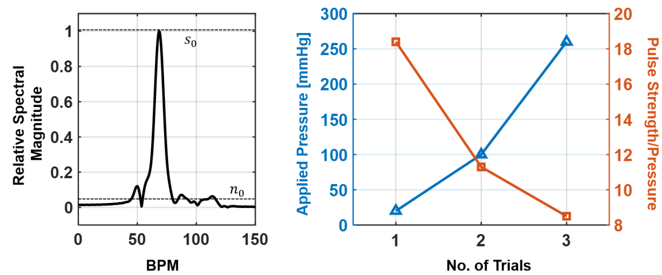

Fig. 8. Radar differential pulse strength/pressure measurement as a result of varying applied external pressure.

$$\begin{aligned} &\text{minimize} \sum_o \sum_m \left\| \partial_t \left[u^{+}_{m,o}(t) e^{-j\omega_o t} \right] \right\|_2^2 \\ &\text{subject to} \sum_o u_{m,o}(t) = \phi_m(t), m = 1, 2, ..., M. \end{aligned} \tag{15}$$

The solution to Eqn. (15) is solved through the Lagrangian-multiplier frame work and the known alternating direction method of multipliers (ADMM) in an iterative fashion. The final solution can be written as the decomposed intrinsic mode functions and the residual signal $r(t)$,

$$\Phi_m(t) = \sum_{o=1}^{O} u^{l+1}_{m,o}(t) + r_m(t), m = 1, 2, ..., M. \tag{16}$$

where l denotes the number of iterations.

VI. Experiment Demonstrations

Our experiment setup includes a millimeter Wave (mmWave) MIMO radar, fingertip oximeter for pulse signal reference, and an arm pressure pump as an external force to change the arm blood flow and consequently the radial arterial pulse pressure. A hand stabling platform is designed to avoid any inevitable hand shake movement during radar measurement as shown in Fig. 5. The measurement site is pre-determined by wrist palpation, which is a common way to feel pulse. Then the boresight of the radar antenna array is aligned with this measurement site as shown in Fig. 5.

In the first experiment example, we demonstrate the surface wrist skin motion extracted from the radar phase by the proposed multi-channel signal processing method. One chunk of measurement is displayed in Fig. 6 compared with the reference pulse. The radar measurement resembles reference pulse waveform.

In the second experiment example, we demonstrate the pulse rate variability analysis for radial artery using radar. This experiment was conducted in a similar setting, however, the test subject was instructed to perform 10 minute cardio physical exercise in order to elevate the heart rate right before the measurement was taken. In this way, we can clearly see the decreasing trend of the relaxing heart rate. The radar measurement well follows this trend and matches with the heart rate calculated from the pulse reference as shown in Fig. 7. A moving slide window with 10 seconds is used to generate the rates in Fig. 7.

In the last experiment example, we showcase the differential radial arterial pulse pressure radar measurement. Absolute blood pulse pressure measurement usually requires external calibration process like seen in conventional cuff based blood pressure device. Indirectly, we use pulse strength variation as a metric to mimic the blood pressure variation because the direct relationship between the measured pulse strength and the blood pressure. The pulse strength is empirically quantified as the ratio of the peak spectral value (s_0) to the estimated noise floor (n_0) as illustrated in Fig. 8. Three measurements were taken for this demonstration. At each measurement, a different external arm pressure was applied and therefore resulted a different arterial pulse strength/pressure. We can see a strong negative correlation among the exerted external pressure and the measured arterial pulse strength/pressure. As the external pressure increases at the upper arm, the radial arterial pulse pressure taken at the same arm decreases. This result consists with our expectation as the high pressure blocks the blood flow and reduces the pulsation at wrist.

VII. Conclusion

We investigated remote assessment of vascular blood flow using radar. We successfully extracted several important biometrics related to the radial arterial blood flow by processing the radar returns. These peripheral site vital sign parameters are pulsation wave, pulse rate, and pulse strength (or relative pressure). More importantly, we conducted pulse rate variability analysis and pulse pressure variability analysis to validate the radar measurements. Our results show the possibility of radar-based remote sensing technology to detect vascular flow changes for screening and diagnosis of peripheral artery diseases.

References

[1] J. C. Lin, "Noninvasive microwave measurement of respiration," *Proceedings of the IEEE*, vol. 63, no. 10, pp. 1530–1530, 1975.

[2] I. Immoreev and T.-H. Tao, "Uwb radar for patient monitoring," *IEEE Aerospace and Electronic Systems Magazine*, vol. 23, no. 11, pp. 11–18, 2008.

[3] Y. Rong and D. W. Bliss, "Remote sensing for vital information based on spectral-domain harmonic signatures," *IEEE Transactions on Aerospace and Electronic Systems*, vol. 55, no. 6, pp. 3454–3465, 2019.

[4] ——, "Is radar cardiography (rcg) possible?" in *2019 IEEE Radar Conference (RadarConf)*. IEEE, 2019, pp. 1–6.

[5] Z. Lei, "Peripheral vascular diseases," 1962.

[6] M. M. Lell, K. Anders, M. Uder, E. Klotz, H. Ditt, F. Vega-Higuera, T. Boskamp, W. A. Bautz, and B. F. Tomandl, "New techniques in ct angiography," *Radiographics*, vol. 26, no. suppl_1, pp. S45–S62, 2006.

[7] P. Hoskins, "Measurement of arterial blood flow by doppler ultrasound," *Clinical physics and physiological measurement*, vol. 11, no. 1, p. 1, 1990.

[8] V. Rajan, B. Varghese, T. G. van Leeuwen, and W. Steenbergen, "Review of methodological developments in laser doppler flowmetry," *Lasers in medical science*, vol. 24, no. 2, pp. 269–283, 2009.

[9] A. Humeau-Heurtier, E. Guerreschi, P. Abraham, and G. Mahé, "Relevance of laser doppler and laser speckle techniques for assessing vascular function: state of the art and future trends," *IEEE transactions on biomedical engineering*, vol. 60, no. 3, pp. 659–666, 2013.

[10] Y. Rong, P. C. Theofanopoulos, G. C. Trichopoulos, and D. W. Bliss, "Cardiac sensing exploiting an ultra-wideband terahertz sensing system," in *2020 IEEE International Radar Conference (RADAR)*. IEEE, 2020, pp. 1002–1006.

[11] N. ur Rehman and H. Aftab, "Multivariate variational mode decomposition," *IEEE Transactions on Signal Processing*, vol. 67, no. 23, pp. 6039–6052, 2019.

[12] K. Dragomiretskiy and D. Zosso, "Variational mode decomposition," *IEEE Transactions on Signal Processing*, vol. 62, no. 3, pp. 531–544, 2013.

[13] P. Cao, H. Wang, and K. Zhou, "Multichannel signal denoising using multivariate variational mode decomposition with subspace projection," *IEEE Access*, vol. 8, pp. 74 039–74 047, 2020.

[14] Y. Rong, K. V. Mishra, and D. W. Bliss, "Multiple moving targets heartbeat estimation and recovery using multi-frequency radars," in *2021 IEEE Radar Conference (RadarConf21)*. IEEE, 2021, in press.